Supporting Information

Theoretical Insights into Electroreduction Mechanism of N_2 to NH_3 from an Improved Au(111)/H_2O Interface Model

Lihui Ou*, Junling Jin*, Yuandao Chen

1. Model and Computational Details

1.1 Surface and Solvation Model

Low-index faceted Au(111) crystal plane is generally chosen as representative surface for experimental studies due to the achieved relatively high Faradaic efficiency to N_2 electrochemical reduction into NH_3.[1] Considering the complexity of real N_2 electroreduction systems, the aqueous-phase environment is included in the present study, in which 12 explicit H_2O molecules with two relaxed bilayer structures chosen to fill up the vacuum region were used to model the solvation effect in order to better simulate the interactions between solvent and adsorbates and decrease the size of the simulated systems as much as possible (See Figure S1). In fact, the formation of an ordered H_2O bilayer structure in a hexagonal arrangement with 2/3 monolayer saturation coverage with respect to the surface normal had been demonstrated by X-ray absorption spectroscopy, thermal desorption spectroscopy, low-energy electron diffraction, X-ray photoelectron spectroscopy and scanning electron microscopy along with DFT calculations in previous experimental and theoretical studies on the meal surface.[2-4] Our present solvation model is on the basis of the previous studies on structure and orientation of H_2O. However, many different H_2O solvation structures may also exist, which all are approximate in energy.[5] Since all energies of interest in this study are energy differences, which are not sensitive to the accurate model of H_2O as long as the same model is consistently used and a reasonable model in a local minimum structure is choose when calculating the energy differences. Considering the coverage is 2/3 of H_2O monolayer, thus, a (3x3) Au(111) slab model with nine metal atoms per layer and theoretical equilibrium lattice constant of 4.16 Å by using four metal layers was created.

*Hunan Province Cooperative Innovation Center for the Construction & Development of Dongting Lake Ecologic Economic Zone, Hunan Provincial Key Laboratory of Water Treatment Functional Materials, Hunan Province Engineering Research Center of Electroplating Wastewater Reuse Technology, College of Chemistry and Materials Engineering, Hunan University of Arts and Science, Changde, 415000, China. E-mail: lihuiou@huas.edu.cn; jinjl174@nenu.edu.cn

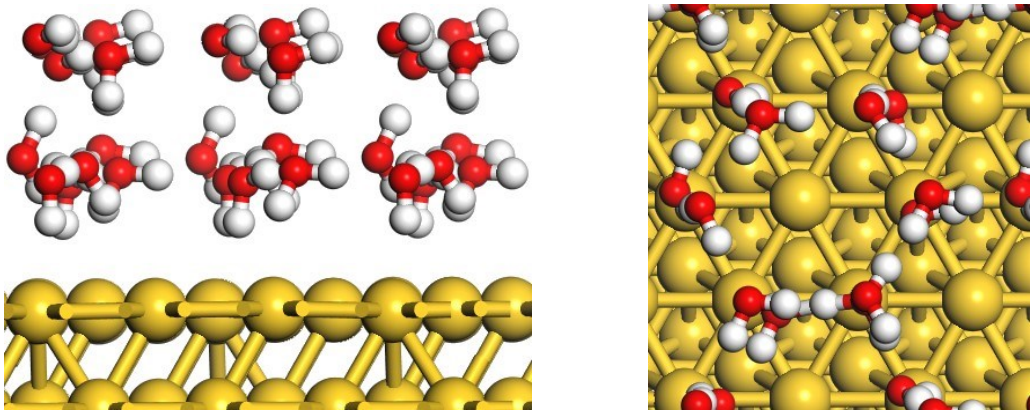

(a) (b)

Figure S1. The solvation model on Au(111) at the electrochemical interface: (a) Side view; (b) Top view.

1.2 Computational Parameters

Using the generalized gradient approximation of the Perdew–Burke–Ernzerhof exchange correlation functional, calculations were performed in the framework of DFT.[6] Ultrasoft pseudopotentials were employed to describe the nuclei and core electrons and the Kohn-Sam equations were self-consistently solved using a plane-wave basis set.[7] A kinetic energy cutoff of 30 Ry and a charge-density cutoff of 300 Ry were used to make the basis set finite. The Fermi surface has been treated by the smearing technique of Methfessel–Paxton with a smearing parameter of 0.02 Ry.[8] The PWSCF codes in Quantum ESPRESSO distribution were employed to perform all calculations.[9] Brillouin-zone integrations were implemented using a (3×3×1) uniformly shifted k-mesh for (3×3) supercell with the special-point technique, which was tested to converge to a subset of the relative energies reported herein. A vacuum layer of 16Å was placed above the top layer of slab, which is sufficiently large to ensure that the interactions are negligible between repeated slabs in a direct normal to the surface. The Au atoms in the bottom two layers are fixed at the theoretical bulk positions, whereas the top two layers and all adsorbates including solvent are allowed to relax to minimize the total energy of the system. Structural optimization was performed until the Cartesian force components acting on each atom were brought below 10^{-3} Ry/Bohr and the total energy was converged to within 10^{-5} Ry. Using the climbing image nudged elastic band (CI-NEB) method, the saddle points and minimum energy paths (MEPs) were located.[10, 11] Zero point energy (ZPE) corrections were applied into the calculations of the activation and reaction energies from MEP analysis, in which density functional perturbation theory within the linear response was used to study the vibrational properties.[12] The ZPEs were calculated using the PHONONS code that contained in the Quantum ESPRESSO distribution.[9]

2. H Adsorption Configuration at Au(111)/H_2O Interface

Various possible surface adsorption sites of H atoms and coverage dependence are considered in our present study, as shown in Figure S2. It is observed that H atoms prefer to adsorb at 3-fold face-centered cubic hollow (fcc) sites at Au(111)/H_2O interface so that they can stay away from each other to minimize the repulsive reactions in our present research scope on θ_H.

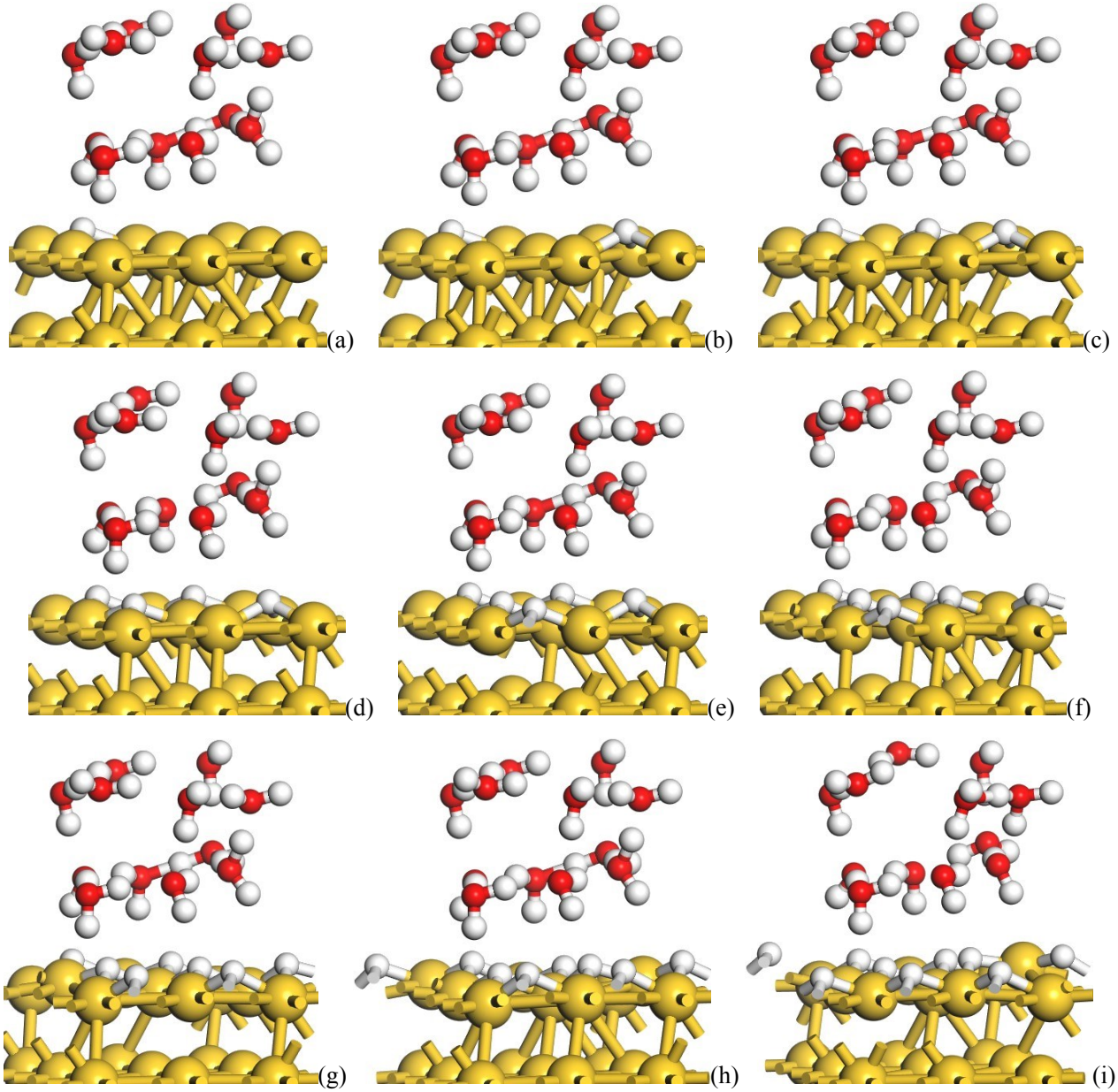

Figure S2. Various possible surface H adsorption configurations at Au(111)/H_2O interface at different H coverage: (a) 1/9 ML; (b) 2/9 ML; (c) 1/3 ML; (d) 4/9 ML; (e) 5/9 ML; (f) 2/3 ML; (g) 7/9 ML; (h) 8/9 ML; (i) 1ML.

3. Images of Reactants, Products and Transition states

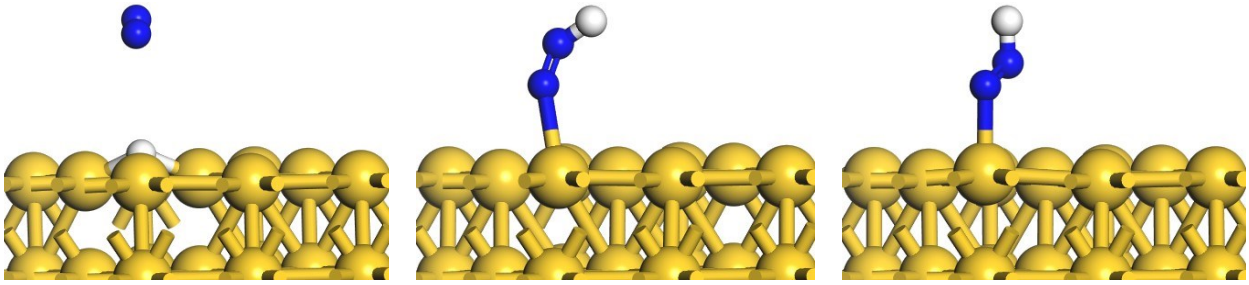

(a) (b) (c)

Figure S3. N_2 reduction into the adsorbed N_2H species via surface hydrogenation on Au(111) in gas phase: (a) Initial state; (b) Transition state; (c) Final state.

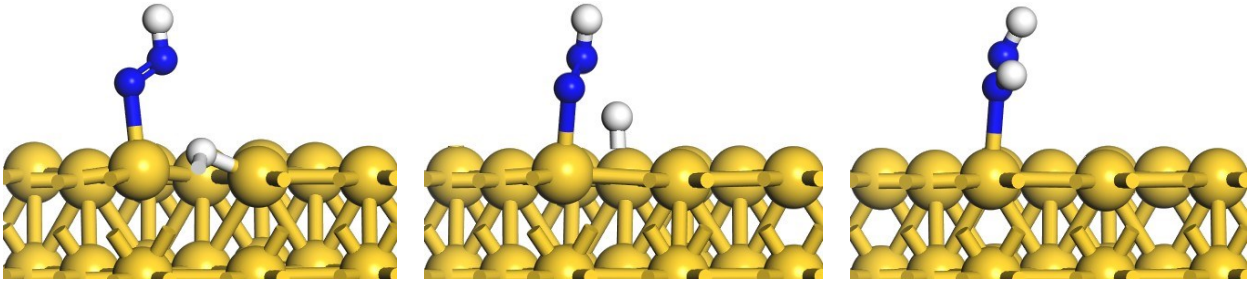

(a) (b) (c)

Figure S4. N_2H reduction into the adsorbed NHNH species via surface hydrogenation on Au(111) in gas phase: (a) Initial state; (b) Transition state; (c) Final state.

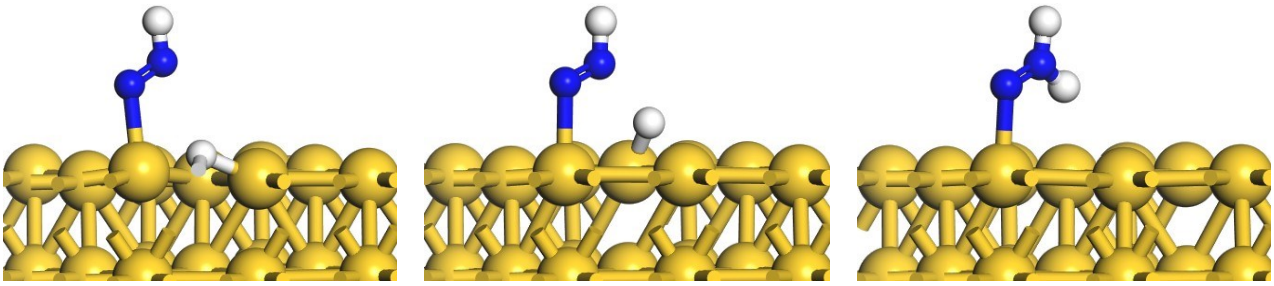

(a) (b) (c)

Figure S5. N_2H reduction into the adsorbed NNH_2 species via surface hydrogenation on Au(111) in gas phase: (a) Initial state; (b) Transition state; (c) Final state.

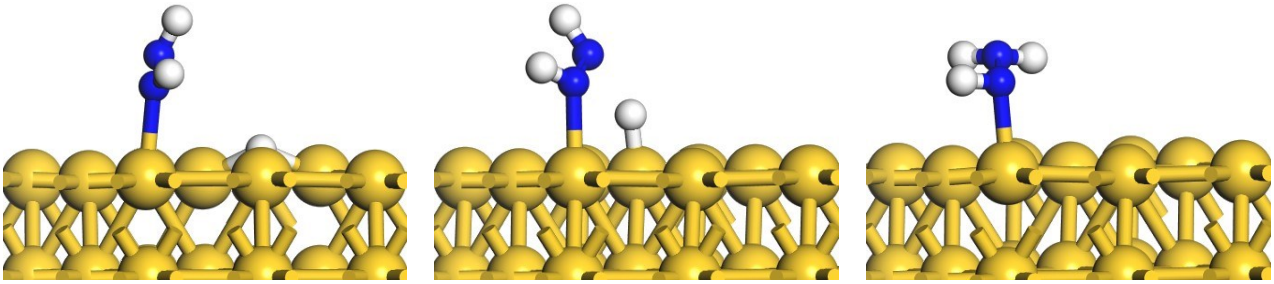

(a) (b) (c)

Figure S6. NHNH reduction into the adsorbed $NHNH_2$ species via surface hydrogenation on Au(111) in gas phase: (a) Initial state; (b) Transition state; (c) Final state.

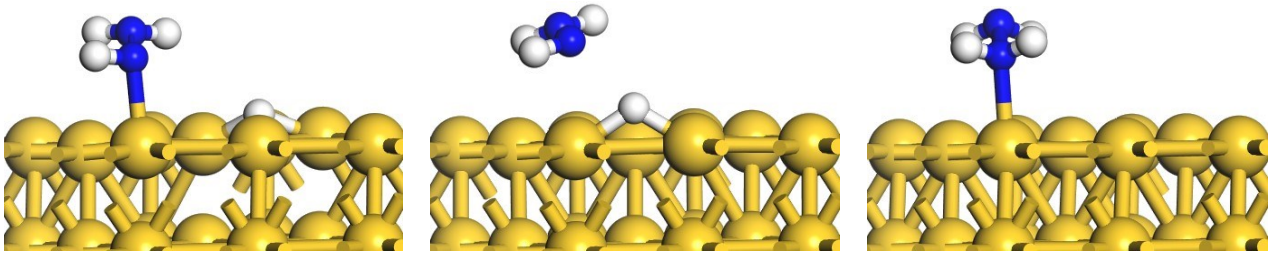

(a) (b) (c)

Figure S7. $NHNH_2$ reduction into the adsorbed NH_2NH_2 species via surface hydrogenation on Au(111) in gas phase: (a) Initial state; (b) Transition state; (c) Final state.

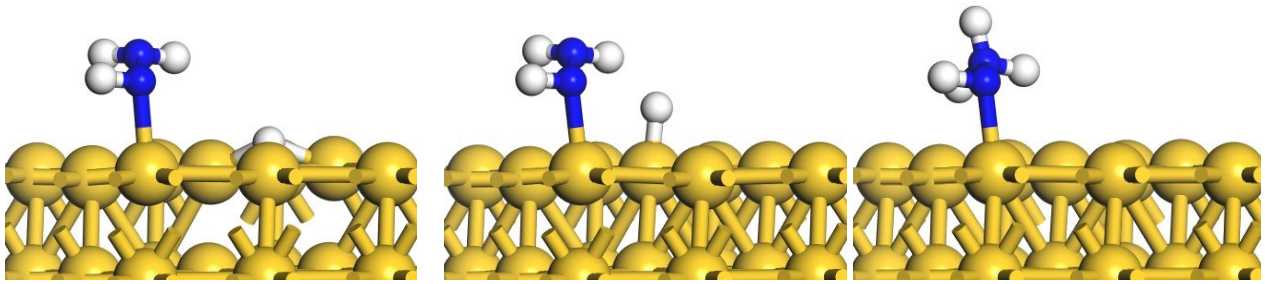

(a) (b) (c)

Figure S8. $NHNH_2$ reduction into the adsorbed $NHNH_3$ species via surface hydrogenation on Au(111) in gas phase: (a) Initial state; (b) Transition state; (c) Final state.

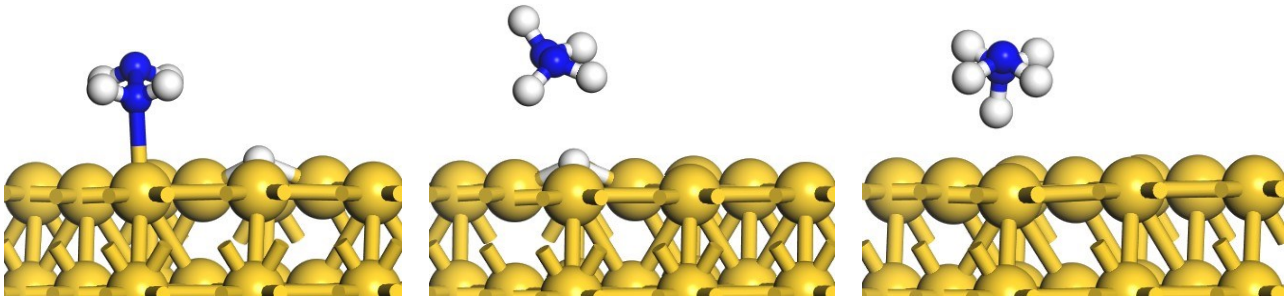

(a) (b) (c)

Figure S9. NH_2NH_2 reduction into the adsorbed NH_2NH_3 species via surface hydrogenation on Au(111) in gas phase: (a) Initial state; (b) Transition state; (c) Final state.

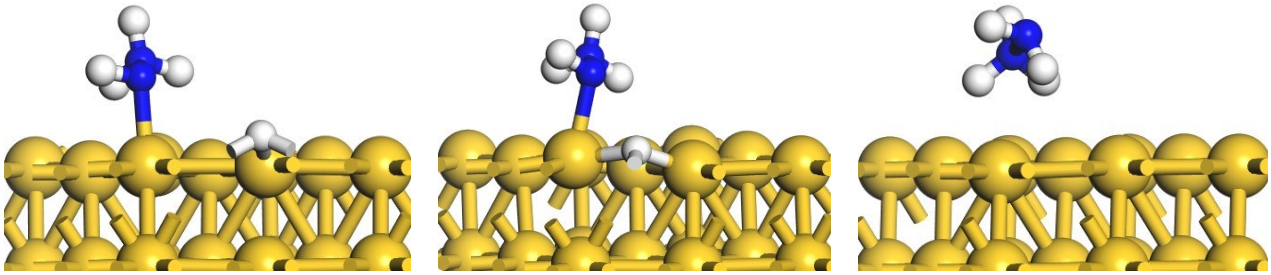

(a) (b) (c)

Figure S10. $NHNH_3$ reduction into the adsorbed NH_2NH_3 species via surface hydrogenation on Au(111) in gas phase: (a) Initial state; (b) Transition state; (c) Final state.

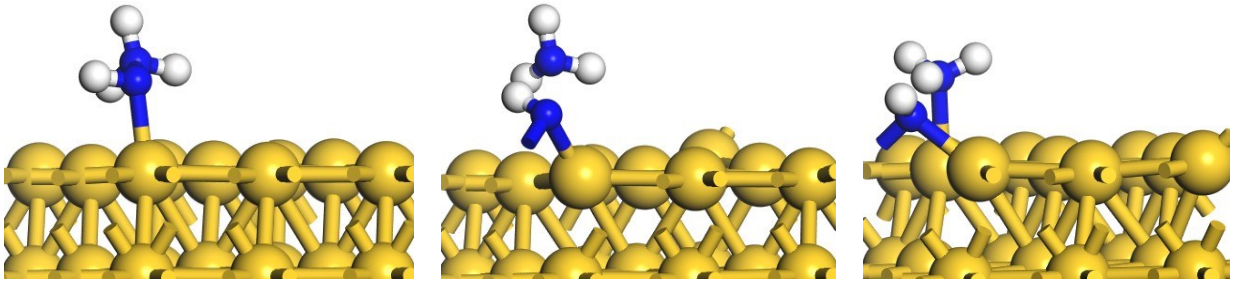

(a) (b) (c)

Figure S11. $NHNH_3$ reduction into the adsorbed NH_2 species and NH_3 product via N-N bond scission on Au(111) in gas phase: (a) Initial state; (b) Transition state; (c) Final state.

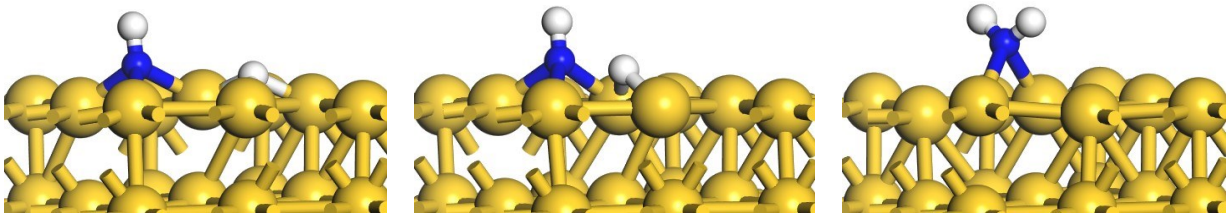

(a) (b) (c)

Figure S12. NH reduction into the adsorbed NH_2 species via surface hydrogenation on Au(111) in gas phase: (a) Initial state; (b) Transition state; (c) Final state.

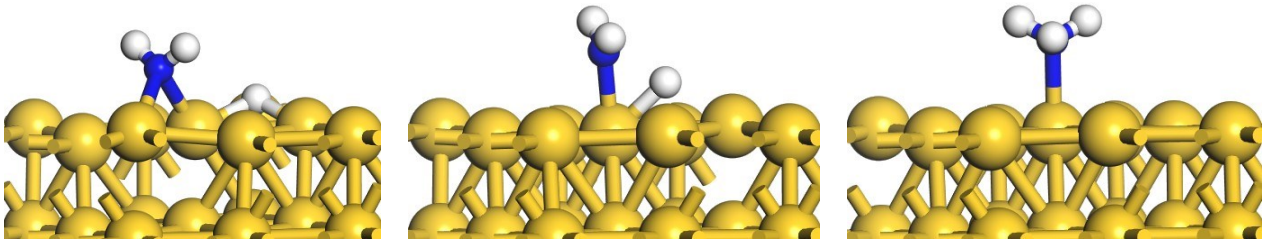

(a) (b) (c)

Figure S13. NH_2 reduction into the adsorbed NH_3 product via surface hydrogenation on Au(111) in gas phase: (a) Initial state; (b) Transition state; (c) Final state.

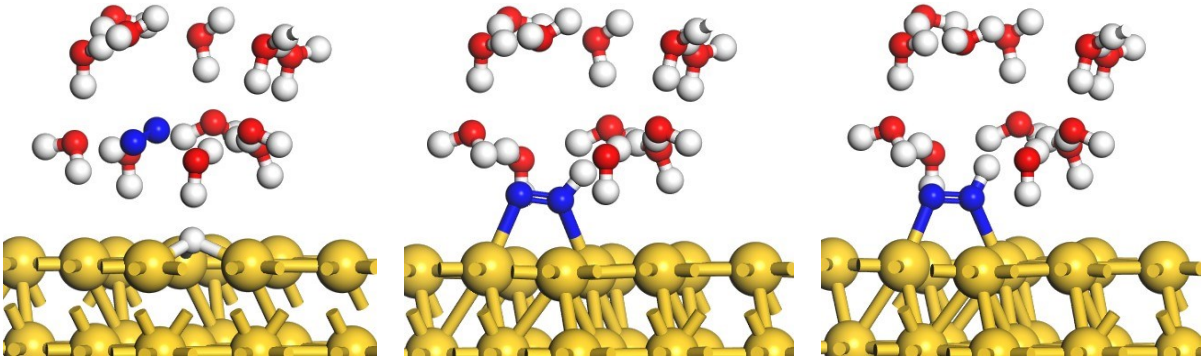

(a) (b) (c)

Figure S14. N_2 electroreduction into the adsorbed N_2H species at the present simulated Au(111)/H_2O interface: (a) Initial state; (b) Transition state; (c) Final state.

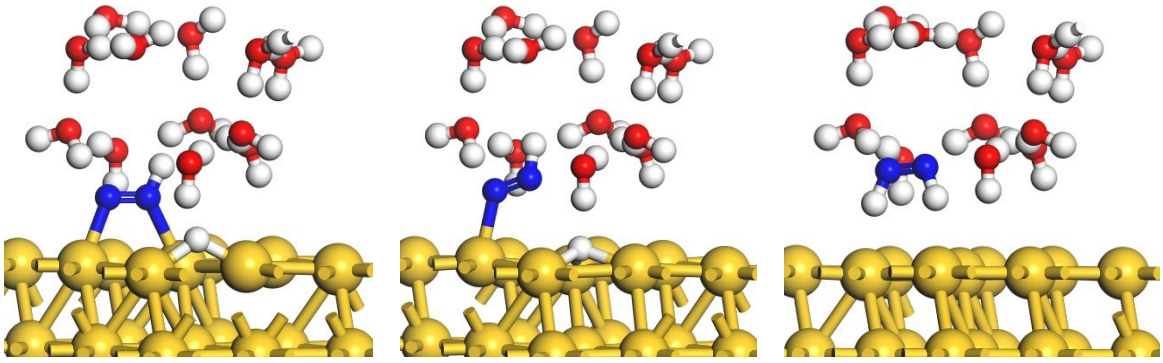

(a) (b) (c)

Figure S15. N_2H electroreduction into NHNH species at the present simulated Au(111)/H_2O interface: (a) Initial state; (b) Transition state; (c) Final state.

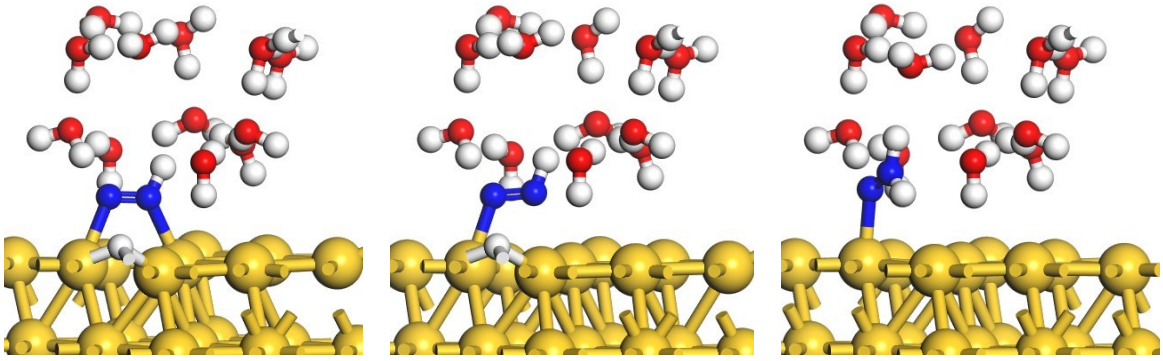

(a) (b) (c)

Figure S16. N_2H electroreduction into the adsorbed NNH_2 species at the present simulated Au(111)/H_2O interface: (a) Initial state; (b) Transition state; (c) Final state.

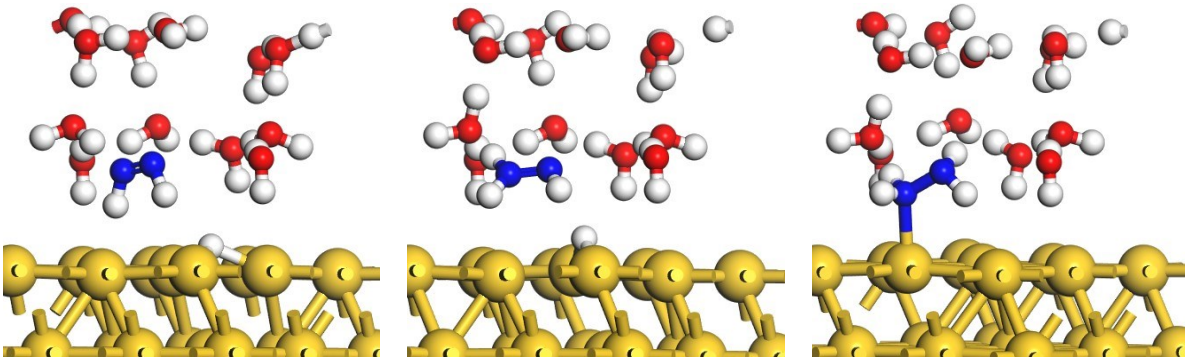

(a) (b) (c)

Figure S17. NHNH electroreduction into the adsorbed NH_2NH_2 species at the present simulated Au(111)/H_2O interface: (a) Initial state; (b) Transition state; (c) Final state.

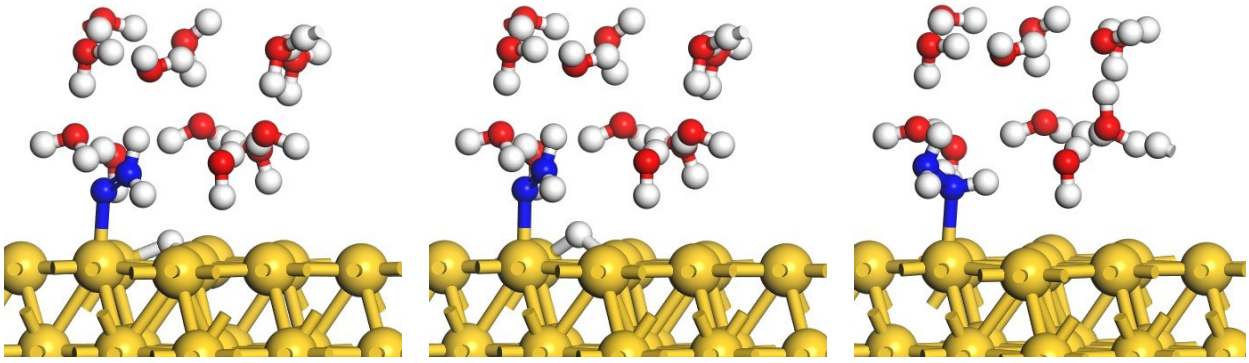

(a) (b) (c)

Figure S18. NNH_2 electroreduction into the adsorbed NH_2NH_2 species at the present simulated Au(111)/H_2O interface: (a) Initial state; (b) Transition state; (c) Final state.

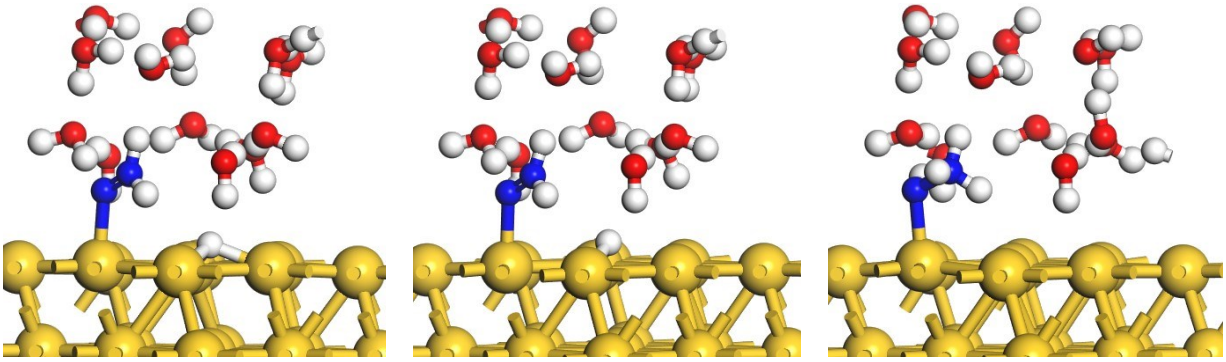

(a) (b) (c)

Figure S19. NNH_2 electroreduction into the adsorbed $NHNH_3$ species at the present simulated Au(111)/H_2O interface: (a) Initial state; (b) Transition state; (c) Final state.

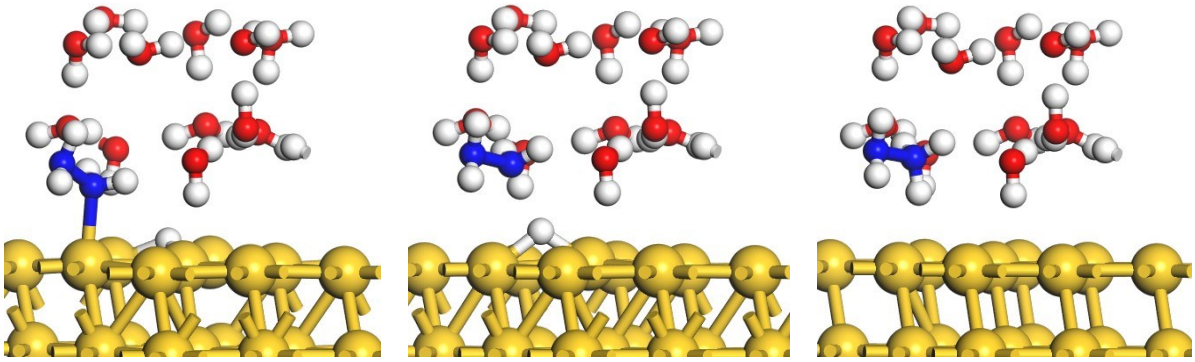

(a) (b) (c)

Figure S20. NH_2NH_2 electroreduction into NH_2NH_3 species at the present simulated Au(111)/H_2O interface: (a) Initial state; (b) Transition state; (c) Final state.

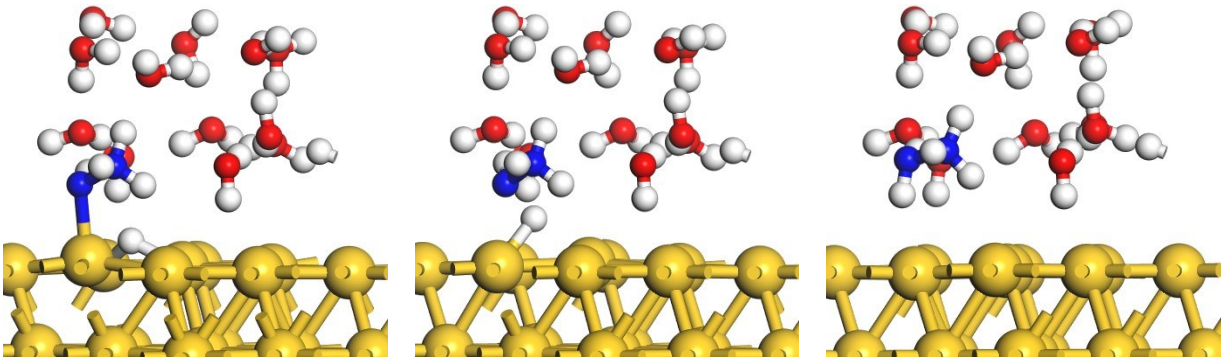

(a) (b) (c)

Figure S21. $NHNH_3$ electroreduction into NH_2NH_3 species at the present simulated Au(111)/H_2O interface: (a) Initial state; (b) Transition state; (c) Final state.

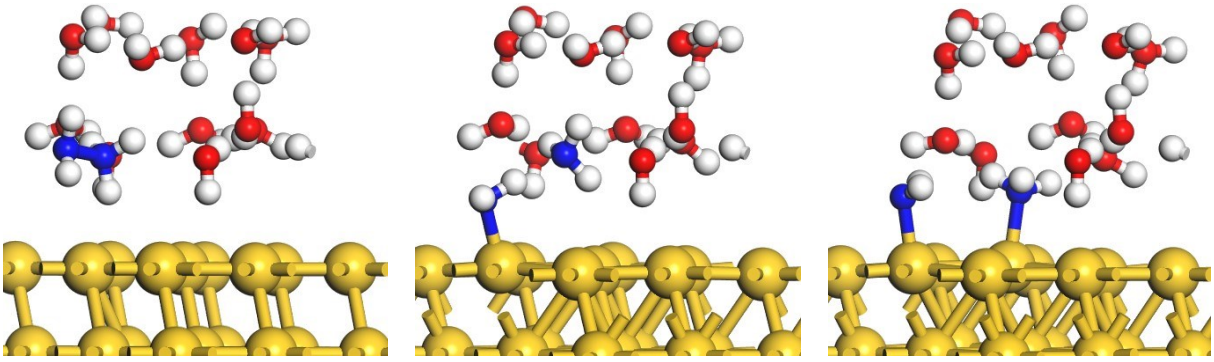

(a) (b) (c)

Figure S22. NH_2NH_3 electroreduction into the adsorbed NH_2 species and NH_3 product via N-N bond scission at the present simulated Au(111)/H_2O interface: (a) Initial state; (b) Transition state; (c) Final state.

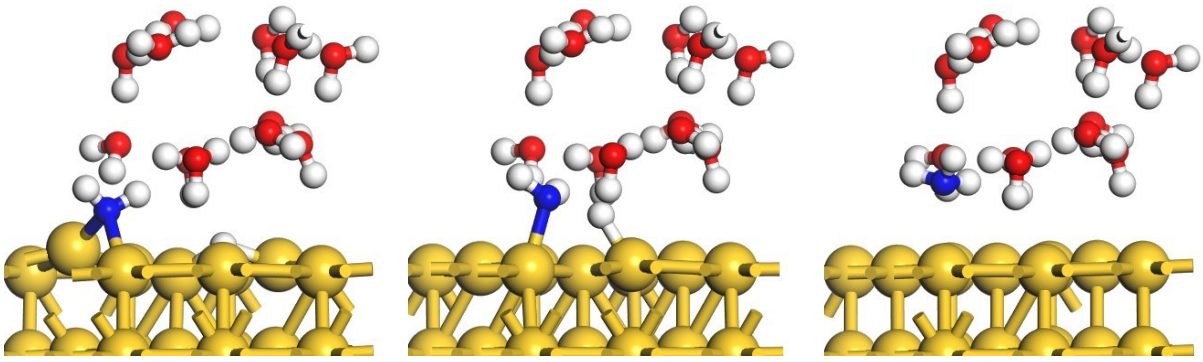

(a) (b) (c)

Figure S23. NH_2 electroreduction into NH_3 product at the present simulated Au(111)/H_2O interface: (a) Initial state; (b) Transition state; (c) Final state.

References

(1) M. Nazemi, S. R. Panikkanvalappil and M. A. El-Sayed, Enhancing the Rate of Electrochemical Nitrogen Reduction Reaction for Ammonia Synthesis under Ambient Conditions Using Hollow Gold Nanocages, *Nano Energy*, 2018, **49**, 316-323.

(2) E. Skúlason, V. Tripković, M. E. Björketun, S. Gudmundsdóttir, G. Karlberg, J. Rossmeisl, T. Bligaard, H. Jónsson and J. K. Nørskov, Modeling the Electrochemical Hydrogen Oxidation and Evolution Reactions on the basis of Density Functional Theory Calculations, *J. Phys. Chem. C*, 2010, **114**, 18182-18197.

(3) M. A. Henderson, Interaction of Water with Solid surfaces: Fundamental Aspects Revisited, *Surf. Sci. Rep*., 2002, **46**, 1-308.

(4) H. Ogasawara, B. Brena, D. Nordlund, M. Nyberg, A. Pelmenschikov, L. G. M. Pettersson and A. Nilsson, Structure and Bonding of Water on Pt(111), *Phys. Rev. Lett*., 2002, **89**, 276102.

(5) S. Haq, C. Clay, G. R. Darling, G. Zimbitas and A. Hodgson, Growth of Intact Water Ice on Ru(0001) between 140 and 160 K: Experiment and Density-Functional Theory Calculations, *Phys. Rev. B*, 2006, **73**, 115414.

(6) J. P. Perdew, K. Burke and M. Ernzerhof, Generalized Gradient Approximation Made Simple, *Phys. Rev. Lett*., 1996, **77**, 3865-3868.

(7) D. Vanderbilt, Soft Self-Consistent Pseudopotentials in a Generalized Eigenvalue Formalism, *Phys. Rev. B*, 1990, **41**, 7892-7895.

(8) M. Methfessel and A. T. Paxton, High-Precision Sampling for Brillouin-Zone Integration in Metals. *Phys. Rev. B*, 1989, **40**, 3616-3621.

(9) S. Baroni, A. Dal Corso, S. de Gironcoli and P. Giannozzi, PWSCF and PHONON: Plane-Wave Pseudo-Potential Codes, http://www.quantum-espresso.org/, **2001**.

(10) G. Henkelman and H. Jonsson, Improved Tangent Estimate in the Nudged Elastic Band Method for Finding Minimum Energy Paths and Saddle Points, *J. Chem. Phys*., 2000, **113**, 9978-9985.

(11) G. Henkelman, B. P. Uberuaga and H. Jonsson, A Climbing Image Nudged Elastic Band Method for Finding Saddle Points and Minimum Energy Paths, *J. Chem. Phys*., 2000, **113**, 9901-9904.

(12) S. Baroni, S. Gironcolli, A. Corso and P. Giannozzi, Phonons and Related Properties of Extended Systems from Density Functional Perturbation Theory, *Rev. Mod. Phys*., 2001, **73**, 515-562.